INVERSION OF HYDROLOGICAL TRACER TEST DATA USING TOMOGRAPHIC CONSTRAINTS

Niklas Linde,[1] Stefan Finsterle,[2] Susan Hubbard.[2]

[1]Department of Earth Sciences/Geophysics, Uppsala University, Uppsala, Sweden.

[2]Earth Sciences Division, Lawrence Berkeley National Laboratory, Berkeley, California.

ABSTRACT

A reasonable description of the hydraulic conductivity structure is a prerequisite for modeling contaminant transport. However, formulations of hydrogeological inverse problems utilizing hydrogeological data only often fail to reliably resolve features at a resolution required for accurately predicting transport. Incorporation of geophysical data into the inverse problem offers the potential to increase this resolution. In this study, we invert hydrological tracer test data using the shape and relative magnitude variations derived from geophysical tomographic data to regionalize a hydrogeological inverse problem in order to estimate the hydraulic conductivity structure. Our approach does not require that the petrophysical relationship be known a-priori, but that it is linear and stationary within each geophysical anomaly. However, tomograms are imperfect models of geophysical properties and geophysical properties are not necessarily strongly linked to hydraulic conductivity. Therefore, we focus on synthetic examples where the correlation between radar velocity and hydraulic conductivity, as well as the geophysical data acquisition errors, are varied in order to assess what aspects of the hydraulic conductivity structure we can expect to resolve under different conditions. The results indicate that regularization of the tracer inversion procedure using geophysical data improves estimates of hydraulic conductivity. We find that even under conditions of

corrupted geophysical data, we can accurately estimate the effective hydraulic conductivity and areas of high and low hydraulic conductivity. However, given imperfect geophysical data, our results suggest that we cannot expect accurate estimates of the variability of the hydraulic conductivity structure.

1. INTRODUCTION

Hydrogeological variability exerts a major control on the movement of solutes in the subsurface, a variability that is often modeled using a blocked (e.g., Carrera and Neuman, 1986a, b, c) or a geostatistical approach (e.g., Hoeksema and Kitanidis, 1984). However, solving hydrogeological inverse problems using hydrogeological data only often leads to non-unique or overly smooth models. McLaughlin and Townley (1996) in their reassessment of the groundwater inverse problem of estimating variations in hydraulic conductivity from point measurements of hydraulic conductivity and head data note that a small number of other variables (such as solute concentration) might be more valuable than just adding additional head data. Also, they state that geophysics offer attractive possibilities to supplement traditional borehole data. An example of the potential use of geophysics in hydrogeological applications is provided by Scheibe and Chien (2003), who perform flow modeling of tracer test data from Oyster, VA. They show that a hydraulic conductivity structure estimated using both radar velocity and hydraulic conductivity data significantly improved transport predictions compared to estimates obtained only from hydraulic conductivity data.

Although the potential benefits of including geophysical data in the estimation of hydrogeological properties have been demonstrated in recent years, there are many obstacles that prohibit the routine use of such data in a quantitative manner. On one hand,

we have minimally-invasive, densely sampled, and relatively cheap geophysical measurements. On the other hand, we have (1) a lack of direct and universal relationships between hydrogeological and geophysical properties, (2) space-varying resolution of geophysical methods, (3) inversion artifacts caused by measurement errors, and (4) smoothness of the inverted geophysical structure estimates that complicate the use of geophysical data in hydrogeological parameter estimation (e.g., Hubbard and Rubin, 2004). Most high-resolution hydrogeological parameter estimation research to date has been carried out using crosshole tomographic methods, most notably using seismic (e.g., Copty et al., 1993; Hyndman et al., 1994; Prasad, 2003), radar (e.g., Chen et al., 2001; Alumbaugh et al., 2002), and electrical resistance tomography (e.g., Daily et al., 1992; Daily et al., 2004). Examples of hydrogeological parameter estimation using tomographic data include estimation of: the hydraulic conductivity and geometry of hydrofacies (McKenna and Poeter, 1995; Hyndman and Gorelick; 1996; Tronicke et al., 2004 (only geometry)); the hydraulic conductivity structure (Hubbard et al., 2001) and its spatial correlation (Hubbard et al., 1999); sediment geochemistry (Chen et al., 2004); moisture content (Alumbaugh et al., 2002); fracture geometry (Slater et al., 1997); infiltration (Binley et al., 2002); and solute transport monitoring (Slater et al., 2002; Day-Lewis et al., 2003). The majority of these studies have assumed that the relationship between a geophysical attribute estimate and a hydrogeological property is stationary, and is as well independent of data acquisition errors and inversion method. In reality, these conditions are rarely met because of two reasons. First, petrophysical relationships are typically non-stationary. Although researchers have tended to define a single petrophysical model to represent the entire area of investigation, in reality these relationships may vary as a

function of hydrogeological heterogeneity. For example, Prasad (2003) illustrated using a real dataset how seemingly uncorrelated measurements of seismic velocity and hydraulic conductivity may have correlation factors as high as 0.9 if they are grouped into hydrogeologically similar units. This means that (1) the estimated petrophysical relationship may be unnecessarily weak if data from different hydrofacies are grouped together in the estimation process or (2) that a petrophysical relationship estimated using data from one type of hydrogeological unit may not be valid for other nearby units. The second reason why conditions are not met is that the tomogram itself is an estimate of the geophysical attribute rather than a precise visualization of the true geophysical structure. The tomogram is affected by many factors including the aspect ratio, data errors, the inversion procedure, and geological heterogeneity (Peterson, 2001; Alumbaugh et al., 2002). The effects of the inversion procedure is illustrated by Day-Lewis and Lane (2004), who show how a perfect linear relationship between radar velocity and hydraulic conductivity deteriorates during the inversion process, and that the tomograms are smooth estimates with a space-varying resolution. Inclusion of tracer test data in the hydrogeophysical estimation process may minimize the influence of inversion artifacts. Furthermore, it allows the simultaneous estimation of the petrophysical relationship at the scale of interest. Hence, making borehole data less important and avoiding the assumption of scale invariance that is needed to apply petrophysical relationships developed at a smaller scale, e.g., through analysis of core samples in a laboratory. Hyndman et al. (1994) jointly inverted synthetic seismic and tracer test data in 2-D to estimate the hydraulic conductivity and geometry of hydrofacies. Hyndman and Gorelick (1996) extended this analysis to 3-D and three unique lithological classes and applied

their method to the Kesterson aquifer, Ca. They observed reasonably good data fit to the tracer test data. Hyndman et al. (2000) established a linear field scale petrophysical relationship between seismic velocity and hydraulic conductivity using tracer test data. Their relationship between seismic velocity and hydraulic conductivity had a correlation factor of 0.74, which can be compared with a relationship of 0.16 using borehole data. The tracer test data were better explained when the hydraulic conductivity realizations were performed using both hydraulic conductivity and seismic traveltime data compared with only hydraulic conductivity data.

We propose a robust method to estimate the hydraulic conductivity structure using tracer data and tomograms without assuming a stationary petrophysical relationship, or stationary geophysical and hydrogeological structures. Our method is general, but we choose to focus on crosshole radar data. To regionalize the inverse problem, we invert hydrological tracer test data using the shape and relative magnitude variations given by geophysical attribute variations, which we refer to herein as anomalies, derived from tomographic data. The quality of the available data and the unknown petrophysical relationship will determine what aspects of the conductivity structure we can estimate. Our estimation procedure has the following priorities in descending order: (1) to capture the mean hydraulic conductivity; (2) to capture high and low hydraulic conductivity zones while avoiding the introduction of false zones; and (3) to capture the spatial variability of the hydraulic conductivity structure. Compared with Hyndman et al. (1994) and Hyndman and Gorelick (1996) we focus on radar data and at estimating a linear petrophysical relationship, and not at estimating values of geophysical attributes that delimit different hydrofacies. This is similar to what Hyndman et al. (2000) did using

seismic and tracer test data, even though we estimate different relationships in different parts of the model. However, the major differences compared with these studies are in the questions we ask, see below.

We use a synthetic model with characteristics similar to the Oyster site (Hubbard et al., 2001) to simulate and invert a large number of data sets that have different degrees of correlation between radar velocity and hydraulic conductivity, as well as different errors in the acquisition geometry and zero-times. We also consider non-stationary petrophysical relationships. We address the following questions:

- Under what conditions can we accurately estimate the petrophysical relationship and can we accurately estimate different petrophysical relationships within the model?
- How is the correlation between our estimated and true hydraulic conductivity structure affected by the tomographic inversion process, the correlation between geophysical and hydrogeological properties, and different geophysical data acquisition errors?
- Can we correctly estimate the variability of the hydraulic conductivity structure?
- How is the estimated variability of the hydraulic conductivity structure affected by the correlation between geophysical and hydrogeological properties and by different geophysical data acquisition errors, such as borehole deviations or misplacement of transmitters and receivers?
- Is a sequential deterministic inversion approach appropriate when the petrophysical relationships and the geophysical data have non-random errors?

In section 2 we describe the inversion approach and define a set of evaluation criteria. In section 3 we evaluate a set of synthetic cases where we consider different correlation factors of the petrophysical relationship and different types of geophysical data acquisition errors. Finally, in section 4 we use the results from section 3 to discuss and draw conclusions with regard to the questions raised above. We also provide an outlook towards methods that could address some of the shortcomings of the present method.

2. METHOD

In this section, we describe the general ideas and assumptions behind our inversion approach, discuss the geophysical and tracer datasets that are used in the inversion procedure, and develop a set of evaluation criteria of the inversion results.

Let us define $Y=\log K$, where K (m/s) is the hydraulic conductivity and log refers to a base of 10. We consider isotropic hydraulic conductivities, we use $\boldsymbol{Y}$ to indicate a matrix with all Y values in the flow model (i.e., $\boldsymbol{Y}$ is not a hydraulic conductivity tensor), and $\hat{\boldsymbol{Y}}$ to indicate the estimated hydraulic conductivity structure. Let $\boldsymbol{V}$ define the true geophysical structure and $\hat{\boldsymbol{V}}$ our tomographic estimate. In this study, we consider radar traveltime data. However, we stress that the framework that we develop is general and could be applied to any geophysical data set. Let $f(Y,V)$ denote the petrophysical relationship between Y and V, hereafter referred to as the intrinsic relation, and $f(\hat{Y},\hat{V})$ denote the petrophysical relationship between $\hat{Y}$ and $\hat{V}$, hereafter referred to as the empirical relation. Let $\rho(Y,V)$ and $\rho(\hat{Y},\hat{V})$ denote the corresponding linear correlation factors. We use the terms intrinsic correlation and empirical correlation to refer to these linear correlation factors.

Our approach is based on the following assumptions:

1. Major variations in the true hydraulic conductivity structure are associated with variations in our estimates of the velocity structure, but variations in the velocity structure may not necessarily correspond to variations in the hydraulic conductivity structure;
2. The variability within anomalous zones of the estimated velocity structure carries hydrogeological information; and
3. A stationary empirical linear relation is applicable within each anomalous zone.

Our inversion approach can be summarized in the following steps: First, we define geophysical anomalies and their internal variability; second, we fit tracer test data by perturbing initial hydraulic conductivity values at pixels that belong to the different geophysical anomalies in order to estimate a hydraulic conductivity structure; and finally we evaluate the estimated hydraulic conductivity model. A detailed description follows below.

2.1 Tomographic anomalies

In this study, we rely on information obtained from high resolution geophysical surveys, such as crosshole radar or seismic velocity datasets. In section 3, we will explore the use of information obtained from synthetic radar velocity fields of varying quality. In all cases, we assume that the radar wave raypaths are straight. For the inversion, we use the travel time associated with the difference between the pick of the first arrival energy and what is called the "zero-time", or the time associated with signal initiation. Our radar velocity contrasts are on the order of 10%; the straight-wave approximation is therefore valid (Peterson, 1986; Gritto et al., 2004). We use the algebraic reconstruction technique (ART) for the tomographic inversion (Peterson et al., 1985). We discretize the

tomograms with uniform pixel sizes that are comparable to the expected resolution in areas with the highest ray density. The number of iterations in the tomographic inversion of synthetic radar data is optimized such that we minimize a weighted L1-norm Φ_V of the deviations between the true and the estimated velocity structure

$$\Phi_V = \sum_{i=1}^{NZ} \sum_{j=1}^{NX} \frac{\left| V_{ij} - \hat{V}_{ij} \right|}{\Theta_{ij}} \Delta_{ij}, \tag{1}$$

where NZ and NX is the number of pixels in the z- and x-direction of the tomogram, respectively; $\boldsymbol{\Theta}$ contains the relative ray intensity at each pixel, where the highest ray intensity is given a value of 1; and Δ_{ij} is 1 if the relative ray intensity for the corresponding pixel is above a certain threshold, otherwise it is 0. The choice of the objective function is related to our hydrogeological inversion, which will be described in section 2.3. High-quality data allow many iterations and we can fit finer features of the data, whereas too many iterations for noisy data will fit the noise and thereby introduce inversion artifacts. Obviously, the optimal number of iterations is unknown in real applications, but the number of iterations is not too important as long as we are reasonably close to the optimal number of iterations (Peterson, 1986). In real applications, the number of iterations is often qualitatively based on the estimated quality of the data and the resulting tomograms.

A tomogram typically has a number of anomalous zones where the tomographic attribute is quite distinct from surrounding areas. These different anomalous zones might correspond to different hydrofacies and be associated with different intrinsic relations. We use the following automated procedure to divide the tomograms into different anomalies:

1. calculate the median $\hat{V}_{median}$ of the estimated velocity structure;
2. assign +1 and -1 to all tomographic pixels that are above or below the median, respectively, and that have a relative ray intensity above a certain threshold (in our study 0.25);
3. group the pixels into different anomalies *u*, such that no pixel has a neighboring pixel with the same type (+1 or –1) that does not belong to the same anomaly, and where each pixel is defined to have eight neighboring pixels (except at the boundaries);
4. discard anomalies that consist of few pixels (in our study less than three);
5. for each pixel, calculate the absolute deviation from the median and multiply this value with the pixel's relative ray intensity divided by the highest ray intensity within that anomaly θ_u^{max};
6. within each anomaly, assign 1 to the largest value calculated in Step 5, and scale all other pixels in that anomaly linearly to a value α_{ij}, which falls between 0 and 1;
7. for each pixel, write the relative magnitude (α_{ij} calculated in Step 6), its location (*i* and *j*) and the anomaly number (*u)* to a file.

We scale the data with regard to the relative ray intensities in order to give less weight to data with poor ray coverage, where we expect a poorer resolution and more inversion artifacts compared to areas where the relative ray intensity is close to 1 (e.g., Day-Lewis and Lane, 2004). We discard anomalies with few cells to keep the number of model parameters as small as possible and because such small anomalies are likely to have an insignificant impact on flow and transport. Other criteria than deviations from the median are necessary in certain cases. Figure (1a) illustrates typical delineations of radar

velocities into different anomalies; Figure (1b) illustrates the distribution of the relative magnitudes α_{ij} within each anomaly.

We also explore an alternative approach to group the data, which is based on the assumption that the empirical relation is constant throughout the model domain. In this stationary case, we in effect have only one anomaly in the entire plane of investigation. To perform this, we:

1. calculate the median of the estimated velocity structure;
2. for each pixel, multiply the deviation from the median with the pixel's relative ray intensity;
3. scale the data linearly such that the largest positive value is 1 and the median is 0;
4. for each pixel, write the relative magnitude (α_{ij} calculated in Step 3) and its location (i and j) to a file.

Figure (1c) illustrates the distribution of α_{ij} using this approach. This figure shows that the relative magnitudes are related to each other and that certain relative magnitudes are negative when only one empirical relation is assumed. Note the difference to Figure (1b), where several empirical relations are assumed, giving positive relative magnitudes only related to pixels in the same anomaly.

The next step is to carry out the hydrogeological inversion to estimate the relationship between the relative magnitudes and the hydraulic conductivity within each anomaly for the case of multiple empirical relations, or for the whole model domain for the case where we assume that the empirical relation is stationary.

2.2 Model parameters

The model vector $\boldsymbol{m}$ in the hydrogeological inversion is

$$\boldsymbol{m} = \left[Y_b, \beta_1, ..., \beta_u, ..., \beta_U, l_1, ..., l_n, ..., l_N\right], \tag{2}$$

where Y_b is a background hydraulic conductivity from which we calculate deviations; β_u is the logarithm of the uth anomaly's perturbation factor (always positive); l_n is the nth sampler's logarithm of its loss factor (explained below). We calculate an estimated value of hydraulic conductivity $\hat{Y}_{ij}$ by

$$\hat{Y}_{ij} = Y_b + \log\left[1 + \left(\beta_{\Gamma_{ij}} - 1\right)\alpha_{ij}\right], \tag{3}$$

where Γ_{ij} is an integer that identifies the estimated anomaly u for this pixel. Equation (3) allows us to handle both positive and negative empirical relations, it avoids negative hydraulic conductivities, and it provides unbiased sensitivity estimates when calculating the Jacobian. We note that our estimated hydraulic conductivity at pixel ij equals the background hydraulic conductivity if $\beta_{\Gamma_{ij}}$ is 1 or if if the relative magnitude α_{ij} is 0; $\beta_{\Gamma_{ij}}$ values close to zero correspond to a low hydraulic conductivity, and large $\beta_{\Gamma_{ij}}$ values correspond to large values. However, equation (3) breaks down when we only seek one empirical relation. This occurs because certain relative magnitudes a_{ij} are negative in that case. We reformulate the calculation of an estimated value of hydraulic conductivity for cases where the relative magnitude a_{ij} is negative such that

$$\hat{Y}_{ij} = Y_b - \log\left[1 + \left(\beta_{\Gamma_{ij}} - 1\right)\left|\alpha_{ij}\right|\right], \tag{4}$$

To account for these potential losses, each sampling location has a loss factor 10^{l_n} with which the simulated mass fraction $\hat{X}_{pn}^{sim}$ at time p and sampling point n is transformed to

$$\hat{X}_{pn}^{sim\,\prime} = 10^{l_n}\,\hat{X}_{pn}^{sim}, \tag{5}$$

where $\hat{X}_{pn}'$ is the transformed tracer mass fraction. The loss factors are the fractions of the tracer that reaches the well at a certain sampling depth. We introduce the loss factors because computing power restricts us from 3-D flow simulations. We note that the loss factor is a good description of the loss of tracer due to flow paths that moves away from the 2-D plane. However, inconsistencies occur if some tracer moves significantly out of the 2-D plane and at a later stage enter the plane again.

2.3 Tracer test data and inversion procedure

The data vector $\boldsymbol{d}$ is defined as

$$\boldsymbol{d} = \left[X_{11}^{obs},...,X_{P1}^{obs},...,X_{pn}^{obs},...,X_{PN}^{obs}\right], \tag{6}$$

where X_{pn}^{obs} is an observed tracer mass fraction in an observation borehole. However, this representation of breakthrough gives no sensitivity to small perturbations of an initial model if the simulated breakthrough curves do not overlap the observed breakthrough curves. Another problem is that there is no way to distinguish between early and late arrivals if the data are treated independently; this leads to local minima. We must either use a global optimization technique or apply time-consuming manual curve fitting procedure before we can apply a local optimization method.

A remedy is to use a two-phase inversion procedure. The first step of this procedure involves fitting an approximation of the integral

$$\int_{t_0}^{t_p} X dt \tag{7}$$

at different times t_p and sampling locations, where t_0 is the time of tracer injection. We then define $\boldsymbol{\Psi}$ as

$$\boldsymbol{\Psi}_{pn}^{obs} = \sum_{i=1}^{p} \left(\frac{X_{in}^{obs} + X_{(i-1)n}^{obs}}{2} \right) (t_i - t_{i-1}), \tag{8}$$

where $\boldsymbol{\Psi}_{pn}^{obs}$ is referred to as the observed cumulative concentration history, and t_i is the time of the ith observation. The simulated concentration history $\boldsymbol{\Psi}_{pn}^{sim}$ is defined in a similar fashion. This representation significantly decreases the number of local minima because the cumulative concentration histories distinguish between early and late arrivals. An example of the cumulative concentration history is shown in Figure (2a), together with the initial response $\boldsymbol{\Psi}_0$ of an initial model vector $\boldsymbol{m_0}$ that is too far away from the true model to be fitted using a localized optimization algorithm on the tracer mass fractions only. Figure (2b) shows the tracer concentration $\boldsymbol{X}$ that corresponds to this cumulative concentration history. We assume that the errors in the concentration data are normally distributed with zero mean and a standard deviation of s. A good estimate of the standard deviation for the cumulative concentration history s_p^{cum} at time p is

$$s_p^{cum} = \sqrt{\sum_{i=1}^{p} (t_i - t_{i-1}) s}. \tag{9}$$

We justify this measure by the fact that the distance from the origin of a random walk has an expected value of the square root of the sum of the individual steps (Spitzer, 1976), and the accumulation of uncorrelated zero-mean Gaussian errors can be considered a random walk.

As the second phase of the hydrological inversion, we can now use our resultant model from the first phase as an initial model in order to fit the breakthrough data. There are several reasons why we shouldn't use our estimated model from the first stage of the inversion as our final model. First of all, our linear interpolation (equation 8) of the

integral of the breakthrough data (equation 7) introduces errors; measurement errors at early times will have a large effect because they are included at each subsequent data point and there is a low sensitivity to the tails. This means that we would expect some improvement when we fit the concentration breakthrough data in the second phase of the hydrogeological inversion. Furthermore, we can better understand results from error and sensitivity analysis that are based on breakthrough data.

We carry out the hydrogeological inversion using iTOUGH2 (Finsterle, 1999), which we have modified to accommodate the calculation of the cumulative concentration histories (equation 8) and our hydraulic conductivity representation (equations 3 and 4). The forward model is calculated using the EOS7 module of TOUGH2 (Pruess et al., 1999). We use the Levenberg-Marquardt minimization algorithm (Marquardt, 1963), where the Jacobian is calculated with forward finite difference quotients for the first few iterations and central finite difference quotients for the last few iterations. Our objective function is defined as

$$\Phi_{cum} = \sum_{i=1}^{P}\sum_{j=1}^{N}\left(\frac{\Psi_{pn}^{sim\,\prime} - \Psi_{pn}^{obs}}{S_{pn}^{1/2}}\right)^2 \tag{10}$$

for the first phase of the inversion and

$$\Phi_{conc} = \sum_{i=1}^{P}\sum_{j=1}^{N}\left(\frac{\boldsymbol{X}_{pn}^{\boldsymbol{sim}\,\prime} - \boldsymbol{X}_{pn}^{obs}}{W_{pn}^{1/2}}\right)^2 \tag{11}$$

for the second phase, where $\boldsymbol{S}$ and $\boldsymbol{W}$ are diagonal matrices of the estimated error variances, i.e., either $(s_p^{cum})^2$ (see equation 9) or s^2. We used 20 iterations for both the first and second phase of the hydrogeological inversion. The number was chosen based on our observation for this study that almost no improvement in the objective function is made after the first ten iterations.

2.4 Definition of evaluation criteria

We define a set of evaluation criteria to facilitate comparisons between different inversion results. The most obvious and typical criterion is the objective function (criterion 1), defined in equation (11). However, due to the non-uniqueness of hydrogeological inverse problems, this is often an insufficient measure. Synthetic modeling allows us to evaluate the performance of the method for different cases using eight additional criteria, defined below.

The pixel-to-pixel correlation between the estimated and true hydraulic conductivity structure is calculated for the region where the relative ray intensities are above the threshold; it is denoted by $\rho(\hat{Y},Y)$ (criterion 2). The effective conductivity, K_{eff} in the direction of the layering of the true hydraulic conductivity structure is calculated using the second-order accurate results derived by Dagan (1989) given by

$$K_{eff} = K_{\mathrm{G}}\left[1 + 2.3 \times \sigma_Y^2\left(\frac{1}{2} - \frac{\lambda}{2}\right)\right], \tag{12}$$

where

$$\lambda = \frac{e^2}{1-e^2}\left[\frac{1}{e\sqrt{1-e^2}}\tan^{-1}\sqrt{\frac{1}{e^2}-1} - 1\right] \text{ and} \tag{13}$$

$e = \dfrac{I_z}{I_x}$, where I_z and I_x are the integral scales in the z- and x-direction, respectively, and K_G is the geometric mean of the hydraulic conductivity. As a performance criterion we also calculate Y_{eff}-$\hat{Y}_{eff}$ (criterion 3), where our estimate of the effective hydraulic conductivity is calculated using $\hat{\sigma}_Y^2$ and $\hat{e}$. In our synthetic examples in section 3, we cannot make a reliable estimate $\hat{e}$ and instead we used e. The reason behind this is that an estimate of the horizontal integral scale $\hat{I}_X$ would be highly uncertain because I_x (1.5

m) is of the same order as the borehole separation (4.2 m). In the synthetic examples in Section 3, we estimated standard deviations in the case-studies using deviations between hydraulic conductivity values that are at least 1.5 m away (6 pixels) from each other in the vertical direction, an offset at which pixels are essentially uncorrelated (I_z is 0.3 m). The estimated standard deviations are normalized by the true standard deviation for comparison (criterion 4).

Another measure that we use to assess the overall similarity between our estimated and true hydraulic conductivity structures is based on the residuals ς (criterion 5), defined as

$$\varsigma\left(\boldsymbol{Y}-\hat{\boldsymbol{Y}}\right)=\frac{1}{NZ\times NX}\sum_{\mathrm{i}=1}^{NZ}\sum_{\mathrm{j}=1}^{NX}Y_{ij}-\hat{Y}_{ij} \tag{14}$$

and the L1-norm (criterion 6), defined as

$$L_1\left(\boldsymbol{Y}-\hat{\boldsymbol{Y}}\right)=\frac{1}{NZ\times NX}\sum_{i=1}^{NZ}\sum_{j=1}^{NX}\left|Y_{ij}-\hat{Y}_{ij}\right|. \tag{15}$$

We estimate the empirical relation within each anomaly u by the following weighted least-squares estimate

$$\hat{\boldsymbol{a}}_{\boldsymbol{u}}=\left(\hat{\boldsymbol{v}}_{\boldsymbol{u}}{}^{\mathrm{T}}\hat{\boldsymbol{v}}_{\boldsymbol{u}}\right)^{-1}\hat{\boldsymbol{v}}_{\boldsymbol{u}}{}^{\mathrm{T}}\hat{\boldsymbol{y}}_{\boldsymbol{u}}, \tag{16}$$

where $\hat{\boldsymbol{v}}_{\boldsymbol{u}}$ consist of $\left(\hat{V}_{ij}-\hat{V}_{median}\right)\frac{\theta_{ij}}{\theta_u^{max}}$ for all $\hat{V}_{ij}$ that belong to anomaly u; $\hat{\boldsymbol{y}}_{\boldsymbol{u}}$ consist of $\left(\hat{Y}_{ij}-\hat{Y}_b\right)\frac{\theta_{ij}}{\theta_u^{max}}$ for all $\hat{Y}_{ij}$ that belong to anomaly u; and superscript T indicates transpose.

Let us define the size ξ_u of anomaly u as

$$\xi_u=\sum_{i=1}^{NZ}\sum_{j=1}^{NX}10^{\left|\hat{Y}_{ij}-\hat{Y}_b\right|}\Omega_{ij}^{u}, \tag{17}$$

where the value of Ω_{ij}^{u} is 1 if the corresponding pixel belongs to anomaly u, otherwise it is 0. We now calculate a weighted norm of variations in $\hat{\boldsymbol{a}}$ (criterion 7) by

$$L_1(\hat{a}_u - \hat{a}_{mean}) = \frac{\sum_{u=1}^{U} \xi_u \left| \hat{a}_u - \hat{a}_{mean} \right|}{\sum_{u=1}^{U} \xi_u}, \tag{18}$$

where the estimated slope of the empirical relation $\hat{a}_{mean}$ is estimated by redefining equation (16) for the whole model domain. We use the estimated slope of the empirical relation normalized by the intrinsic relation as a performance criterion (criterion 8). Finally, we define a measure of how well the loss factors are fitted (criterion 9)

$$L_1(l_i - \hat{l}_i) = \frac{1}{N} \sum_{i=1}^{N} \left| l_i - \hat{l}_i \right|, \tag{19}$$

where $\hat{l}_i$ denotes the ith estimated logarithm of the loss factor.

3. SYNTHETIC EXAMPLES

In this section, we apply our methodology to estimate the hydraulic conductivity structure using tracer breakthrough and radar traveltime data for a set of synthetic examples. We assess the influence of different intrinsic relations and geophysical data errors on our estimates of the hydraulic conductivity structure. We generate the true hydraulic conductivity structure using an unconditional sequential Gaussian simulation (Deutsch and Journel, 1998) with an exponential variogram model and a correlation structure similar to that at the Oyster, VA site (Hubbard et al., 2001). In this case, we used integral scales of I_x=1.5, I_z=0.3, and a standard deviation of σ_Y=0.26 (see Figure 3a). We define the intrinsic relation by scaling the true hydraulic conductivity structure such that the lowest value corresponds to a velocity of 58 m/μs and the highest value to 64

m/μs, which is the range of velocity values observed at the Oyster site (Hubbard et al., 2001). The intrinsic relation is: V(m/μs)=80.6+4.3Y. We can now use the intrinsic relation to map the true hydraulic conductivity structure into the true velocity structure. However, we are not only interested in cases where the intrinsic correlation is perfect. We create a set of radar images $\boldsymbol{V}_k$ that have different intrinsic correlations, but have the same standard deviation and integral scales as the true velocity structure. We do this by generating a new hydraulic conductivity structure $\boldsymbol{Y}_0$ that has the same standard deviation and integral scales as the true hydraulic conductivity structure but has no correlation with the true hydraulic conductivity structure. These two hydraulic conductivity structures allow us to calculate a set of hydraulic conductivity structures that have intermediate correlations by

$$\boldsymbol{Y}_k = \boldsymbol{Y}_0 + k(\boldsymbol{Y} - \boldsymbol{Y}_0), \tag{20}$$

where k=0.0,0.1,…,1.0 and $\boldsymbol{Y}=\boldsymbol{Y}_{1.0}$. For each k we use the intrinsic relation to map the hydraulic conductivity structure onto a velocity structure $\boldsymbol{V}_k$ (see Figure 4).

Hypothetical crosshole radar tomographic surveys of the different velocity structures are carried out using typical spacing of transmitters and receivers (i.e., 30 cm) and different data acquisition errors. We consider errors caused by:

1. incorrect assumptions of the zero-times;
2. random errors in the horizontal position of the sources and receivers;
3. Inaccurate depth information and horizontal separation between boreholes; and
4. dipping boreholes, which were assumed to be vertical.

The errors are chosen to represent ranges of typical errors for high-resolution, local scale surveys (J. Peterson, personal communication, 2004). We restrict the inversions of the

radar data to rays with angles less than 45° because high angle ray-paths traveling through the earth is often distorted by faster rays traveling within the boreholes (Peterson, 2001). The data are inverted using the ART technique, as described in section 2.1. We use each estimate of a velocity structure $\hat{V}_k$ to estimate the anomalous zones and their internal variability as described in Section 2.1. The observed tracer data are obtained by simulating flow and transport through the true hydraulic conductivity structure (Figure 3a) from a 9.3 m line source using a slug test of 280 g bromide. The bromide concentration is synthetically sampled with multi-samplers at every 0.9 m at one vertical borehole every 18 h during 19 days, with an error of 10 ppb. The observed tracer data are shown in Figure 2 and a conceptual model of the sampled domain is shown in Figure 3b. We can compare different estimates of the hydraulic conductivity structure with the true structure visually and by using the different evaluation criteria defined in Section 2.4.

We first verified the implementation of our method by carrying out the hydrogeological inversion for the case where the true velocity structure (not an estimated velocity structure) was used to estimate the anomalies (see Figure 1). We then fit the tracer data within their error levels and recovered the intrinsic relation. A number of cases were subsequently considered (Table 1). We start by considering very small geophysical data acquisition errors and a perfect intrinsic relation (see Case 1), which we gradually degrade (see Cases 2-11). In Cases 12-20 we work with strong intrinsic relations and with different data acquisition errors.

Our first step is to estimate the velocity structure through tomographic inversion for these cases; the results are summarized below and given in Table 1. The anomalies are estimated following the procedures described in section 2.1. For many cases, the

estimated velocity structure yielded the same anomaly type (i.e., above or below the median) as the true velocity structure in approximately 90% of the pixels where the relative ray intensity is above 0.25. This is not the case when the intrinsic correlation decreases (i.e., k in equation 20 is less than 0.5) (see Cases 6-11), when we have large errors in the horizontal offsets of the boreholes (see Case 12), or when borehole deviations exist (see Case 20). The numbers of anomalies are fairly variable between the cases, varying from 3 to 12, with a median of 7. Fewer anomalies are estimated when we consider realistic acquisition errors because we use fewer iterations in the tomographic inversion to minimize the misfit of the observed and simulated travel times (see equation 1). Hence, resolving less features leads to fewer anomalies. The next step is to carry out the hydrogeological inversion as described in sections 2.2-2.4. The hydrogeological inversion is carried out twice for each case: by estimating one empirical relation for each anomaly, or estimating only one empirical relation for the entire model domain. We use the terms "non-stationary" and "stationary" inversion to refer to these two types of inversions, respectively. We use subscripts NS and S to distinguish between the non-stationary and stationary estimates of hydraulic conductivity. The results of the non-stationary inversions tell us if we can estimate the intrinsic relation through variations within velocity structure anomalies and if we can estimate different intrinsic relations. The stationary inversions are used for comparison with the non-stationary inversions, but also to assess the discrepancies between empirical and intrinsic relations.

Below we describe five examples of how the hydraulic conductivity estimates obtained using tracer and geophysical data are affected by (1) the tomographic inversion; (2) non-stationary intrinsic relations; (3) non-random errors in the intrinsic relations; (4)

geophysical data acquisition errors (but no errors caused by unknown borehole deviations); and (5) errors caused by unknown borehole deviations. Subsequently, we use a graphical representation of certain evaluation criteria for a broad range of cases to illustrate the effects of structured noise in the intrinsic relation and errors in the geophysical data acquisition.

3.1 Example 1: Tomographic inversion

We consider the case where the intrincic relation is stationary, the intrinsic correlation is almost perfect, and the geophysical data acquisition errors are unrealistically small (Case 2 in Table 1). We introduce a zero-time error of 0.33 ns and random location errors of the sources and receivers within the boreholes, modeled as independent realizations from a uniform distribution between –2 and 2 cm. This example illustrates the effect of sparse data sampling under very good data acquisition and investigation conditions.

First, our estimated velocity structure (Figure 5a) is a smooth estimate of the true structure (Figure 4a); it captures the major features in the central part of the model area but has problems in the upper and lower parts, as well as close to the boreholes, as has been reported by other researchers (e.g., Day-Lewis and Lane, 2004). The vertical experimental variograms γ_z in Figure 5b show that the estimated velocity structure is considerably less variable than the true hydraulic conductivity structure, where the exponential variogram of the estimated velocity structure has been scaled using the intrinsic relation to be comparable. Using the obtained tomographic anomalies following Section 2.1, tracer test data, and the procedure described in Section 2.3, we estimate the hydraulic conductivity structure. We compare our estimated hydraulic conductivity structures based on the non-stationary (Figure 5d) and stationary (Figure 5e) inversions.

Images of the residuals (Figures 5f and 5g) show that both models are good representations of the true hydraulic conductivity structure with essentially random errors in the central parts of the models. The estimate based on the non-stationary inversion accurately estimates the variability of the true hydraulic conductivity structure (see γ_z in Figure 5b), whereas, the stationary inversion results in an estimate that is even smoother than the estimated velocity structure. This means that the empirical relation is non-stationary even if the intrinsic relation is stationary. It also suggests that the non-stationary inversion can amplify features in the smooth velocity estimate and create a more realistic hydraulic conductivity estimate than a simple mapping of the velocity estimate onto a hydraulic conductivity estimate through an intrinsic relation, even if this relation is known and has a perfect intrinsic correlation.

3.2 Example 2: Influence of non-stationary intrinsic relations

The non-stationary inversion can potentially handle different intrinsic relations in different anomalies. We use the example discussed in Section 3.1 with one difference: the hydraulic conductivity values of one of the anomalies (approximately between 9 and 10 m depth and 0 to 3 m along the *x*-axis in Figure 3a) has been reflected around the median, making the originally low hydraulic conductivity anomaly now hydraulically conductive. Our estimated velocity structure shown in Figure 6a is unchanged compared to the previous example (see Figure 5a). We repeat the hydrogeological inversion using the geophysical and tracer test data. Our estimation of the hydraulic conductivity structure using the non-stationary inversion provides an accurate estimate of the new high hydraulic conductivity anomaly, whereas the stationary inversion models a low hydraulic conductivity zone. The variability of the true hydraulic conductivity structure is preserved

in the inversion estimates based on the non-stationary inversion (Figure 6b) whereas it is even smoother than the previous example (Figure 5c) for the stationary inversion (Figure 6c). The residuals (Figure 6f) based on the non-stationary inversion still show a random pattern, whereas the residuals (Figure 6g) based on the stationary inversion shows a large non-random error at the new hydraulically conductive anomaly.

3.3 Example 3: Weak intrinsic relation

In this example, we consider more realistic correlations between geophysical attributes and hydraulic conductivity. Prasad (2003) report on correlation factors between seismic velocity and permeability as high as 0.9 although Pride (2004) describes how a universal relationship is impossible. There is also no universal relationship between radar velocity and permeability (e.g., Annan, 2004) although site-dependent relationships have been found through links with porosity (Lesmes, 2004). This means that the correlation between radar velocity and permeability might be anything from almost perfectly correlated to not correlated at all. We use $\boldsymbol{V_5}$ as the velocity structure from which we calculate the radar travel time data (i.e., Case 6 in Table 1). Figure 7a shows our estimated velocity structure for this case. We observe differences between the resulting structure and our earlier estimate (Figure 6a). For example, the high velocity zone at 8 m depth in Figure 6a is less pronounced in Figure 7a. The vertical exponential variogram of our estimated hydraulic conductivity structure based on the non-stationary inversion is much too variable (Figure 7b), whereas the variability in the estimate based on the stationary inversion is even smoother than in illustration 1 (Figure 5c). The much too variable estimates based on the non-stationary inversion can also be seen on the residuals (Figure 7f) that are larger than the ones based on the stationary inversion (Figure 7g). In

this case, the non-stationary inversion has the freedom to model different empirical relations for different anomalies, and it will fit "noise" manifested by correlated deviations from a perfect intrinsic relation. We see that both the non-stationary (Figure 7d) and stationary (Figure 7e) inversion estimates are severely deteriorated compared with the true hydraulic conductivity structure (Figure 3a), but that we accurately model major regions with high or low hydraulic conductivity.

3.4 Example 4: Effects of data acquisition errors

It is now time to consider more typical acquisition errors. We use the example of example 1, but we have increased the zero-time error to 1 ns, incorporated a 5 cm error in the depth of the receivers, and a distance between the boreholes that is 10 cm shorter than what is assumed (i.e., Case 19 in Table 1).

ART inversion of the radar travel time data using the incorrect geometry information yielded a velocity range of 60 to 66 m/μs, instead of the true range of 58 to 64 m/μs. If we used this estimate together with a relation established from theoretical considerations or laboratory experiments to estimate the hydraulic conductivity structure we would create an estimate imaged around the wrong background hydraulic conductivity. Using this biased radar velocity structure, we again performed our hydrogeological inversion. The estimated hydraulic conductivity structure based on the non-stationary inversion (Figure 8d) and the one based on the stationary inversion (Figure 8e) are centered around the background hydraulic conductivity. This example highlights the advantage of including geophysical and tracer data in an inverse procedure even if the geophysical dataset is corrupted. The optimal number of tomographic iterations was 10, not 35 as in the previous examples. This explains why our estimated velocity structure is smoother

(Figure 8b) compared to previous examples. Our estimates of the hydraulic conductivity structure do not resolve a lot of detail within the anomalies, but the anomalies are well placed, as evidenced by the residuals (Figure 8f and 8g). The estimate based on the non-stationary inversion is more variable than the estimated velocity structure (see Figure 8b), whereas the estimate based on the stationary inversion is smoother (Figure 8c). We note that these geophysical data acquisition errors lead to smoothing but do not create any significant bias or inversion artifacts in our estimates of the hydraulic conductivity structure.

3.5 Example 5: Borehole deviations from vertical

Our last example is the same as example 1, but with a 2% deviation of the right borehole while it is assumed that the borehole is vertical (i.e., Case 20 in Table 1). Based on analysis of borehole deviation logs at hydrogeological study sites, deviated wellbores are a norm rather than an anomaly. Our current practice is to collect borehole deviation logs with all high resolution tomographic datasets to account for these potential errors. Under the error conditions in this example, our estimated velocity structure has too high radar velocities and it is severely distorted, e.g., the high velocity zone at the bottom of the tomogram in Figure 9a. Our estimate of the hydraulic conductivity structure based on the non-stationary inversion has by coincidence the correct variability (Figure 9b), but it is not very similar to the true hydraulic conductivity structure (Figure 9d and 9f). Our hydraulic conductivity estimate based on the stationary inversion is an extremely smooth estimate (Figure 9c and 9e) that gives smaller residuals (Figure 9g) than the non-stationary inversion (Figure 9f). We see that unknown borehole deviations have large consequences for our estimation of the hydraulic conductivity structure, and that

deviation logs are needed if any attempts to estimate the hydraulic conductivity structure from an estimated velocity structure should be made.

3.6 Evaluation criteria scores

In the examples presented above we qualitatively illustrated our method's sensitivity to different effects that degrade our estimates of the hydraulic conductivity structure. In this section, we use the evaluation criteria defined in Section 2.4 to identify what happens when the intrinsic relation degrade or if we introduce errors in the geophysical data acquisition (see Table 1). We will also provide figures to illustrate a subset of the criteria defined in section 2.4, including the objective functions (criterion 1), the empirical correlation (criterion 2), the estimated variability (criterion 4), and the mean slope of the empirical relation (criterion 8). Although all criteria are reported in Table 2 for all case studies, we will describe these criteria scores in detail and the figures provide a much better overview.

As shown in Figure 10a, objective functions (equation 11, criterion 1) of the stationary inversions increase approximately linearly on a log-scale when we decrease the intrinsic correlation, while we fit the data equally well for the non-stationary inversions. This indicates over-parameterization of the number of independent empirical relations in the non-stationary inversions. The geophysical data acquisition errors have as large effects as a low intrinsic correlation, where the largest effects are caused by large horizontal errors in the wellbore locations and unknown borehole deviations.

The empirical correlation (criterion 2) decreases approximately linearly (Figure 10b) with decreases in the intrinsic correlation. The highest empirical correlations are observed for the stationary inversions and the highest value is 80%, showing the loss of

information caused by insufficient data sampling and the inversion process that degrade our estimate even if the intrinsic correlation is perfect and data acquisition errors are small. The empirical correlations decrease when we add geophysical data acquisition errors. For example, the 2% error in the borehole deviation (case 20) decreases the empirical correlation to the same level as when the intrinsic correlation is 0.6 and almost no geophysical data acquisition errors are considered. Obviously, the intrinsic correlation is not under our control and it provides an upper limit to the empirical correlation. A careful geophysical survey may result in empirical correlations close to this upper limit but even small acquisition errors give significantly lower correlations with a resulting decrease in the usefulness of our estimates.

The effective hydraulic conductivity is well estimated (Table 2) with mean residuals (equation 12, criterion 3) of 0.052 and 0.022 for the non-stationary and stationary inversions, respectively, showing that the tracer test data constrain the solution around the effective hydraulic conductivity; thus, decrease the effects of inaccurate well locations.

The non-stationary inversions give accurate estimates of the variability (criterion 4) (Figure 10c) when the intrinsic correlation is high, and it is increasingly too variable when the intrinsic correlation decreases. The estimates based on the stationary inversion are too smooth, starting at 75% of the true variability and decreasing linearly to 40% of the true values. Geophysical data acquisition errors give smoother hydraulic conductivity estimates because we use less iterations in the tomographic inversion in order to minimize the misfit of observed and simulated travel times, see equation (1).

The absolute values of the residuals (equation 14, criterion 5) have medians of 0.040 and 0.050 for the non-stationary and stationary inversion, respectively, whereas the L1-

norm (equation 15, criterion 6) have medians of 0.23 and 0.17 for the stationary and non-stationary inversions, respectively.

The stationary inversions give approximately the same slope of the empirical relation (criterion 8) as the intrinsic relation and the non-stationary inversions have higher values that increase as the intrinsic correlations decrease; geophysical data acquisition errors give lower values, i.e., smoother structures. Variations in our empirical relations are substantial (see Table 2, criterion 7) for all cases showing that we cannot estimate intrinsic relations from variations within anomalies of the velocity structure. The variations increase as the intrinsic correlations decrease and as the geophysical data acquisition errors get more severe.

Furthermore, we see that the logarithm of the loss factor (equation 18, criterion 9) is well estimated with a median of 2.75% and 2.3% for the non-stationary and stationary inversion, respectively, meaning that the perturbation factors and the loss factors are weakly correlated.

These results indicate that only our objective function (equation 11, criterion 1) is an insufficient measure of model performance and that it is very difficult too distinguish errors caused by geophysical data acquisition errors or by a low intrinsic correlation and, therefore, to assess the quality of our estimated hydraulic conductivity structure. Laboratory measurements of core samples, geophysical borehole logs, or flow meter data may be highly useful to assess the validity of field estimates.

4. DISCUSSION AND CONCLUSIONS

Our method uses the internal variability of tomographic anomalies to regularize a hydrogeological inverse problem, which we solve using tracer test data in order to

estimate the hydraulic conductivity structure. Our procedure simultaneously yields the empirical relation between the geophysical attributes and hydraulic conductivity. Our focus in this study is not on the method's applicability in a real field setting, but rather on how the estimates of the hydraulic conductivity structure obtained from tracer test data alone can be improved by incorporating geophysical information and how the estimates are affected by the correlation between the geophysical (i.e., radar velocity) and the hydrogeological properties (i.e., hydraulic conductivity), as well as geophysical data acquisition errors. We apply our method to a set of synthetic examples where we vary the intrinsic relation and the geophysical acquisition errors. Our primary findings are summarized as:

1. Geophysical information can constrain hydrogeological inversion, in this case through regularization, making the inverse problem better posed.
2. We can accurately estimate the hydraulic conductivity structure if a good intrinsic relation between geophysical and hydrogeological parameters exists and the geophysical data acquisition errors are very small, even if the identified anomalies have different intrinsic relations (see Figure 6).
3. The incorporation of tracer test data assure that we can accurately estimate the effective hydraulic conductivity even if the intrinsic relation is weak and geophysical data acquisition errors are large (see criterion 3 in Table 2).
4. The correlation between the true hydraulic conductivity structure and our estimates decrease linearly to zero as we decrease the quality of the intrinsic relation (see Figure 10b).

5. Geophysical data acquisition errors significantly decrease the correlation between the true hydraulic conductivity structure and our estimates for a given intrinsic relation (e.g., half of the correlation is lost if we have an unknown borehole deviation of 2%).
6. The non-stationary inversion estimates have the correct variability when the intrinsic relation is high and geophysical data acquisition errors are low, but it is too variable when the intrinsic relation decreases and it is too smooth when geophysical data acquisition errors are more reasonable. The stationary inversion always yields estimates that are too smooth and that get even smoother as the intrinsic relation decrease and the geophysical data acquisition errors increase.
7. The non-stationary inversion is over-parameterized, which is manifested by good data fit even if the intrinsic relation is low and the geophysical data acquisition errors are large (see Figure 10a). This shows that it is in practice difficult to estimate several intrinsic relations given this amount of data.

The results presented in this work indicate an upper limit of what could be obtained in a real field setting for a given petrophysical relationship and geophysical data acquisition errors. This is so because we disregard many sources of errors. For example, we assume a linear petrophysical relationship that is not physically-based; we disregard effects of the ray approximation; we neglect 3-D effects of the flow field and hydrogeological structures smaller than the pixel size; we assume unreasonably small random errors in the hydrogeological data acquisition; and we assume that the test design is perfectly known. We have not considered different designs of the tracer test experiment, but we expect the results to be general. Clearly, we need the tracer to sample a large portion of the aquifer

making a line source or several point sources needed. Furthermore, we have not attempted inversion of the tracer test data without regularization through the tomograms. This would invoke assumptions that we don't want to make, a layered structure or a known correlation structure. However, an example of what we would expect is given by the non-stationary inversion of case 12, where the intrinsic correlation is zero. However, such a comparison is not completely fair because borehole information would probably have been utilized if hydrogeological inversion using hydrogeological data only would have been attempted.

We refer to this method as a sequential deterministic inversion approach because we perform the geophysical inversion independent of the hydrogeological data and we cast the inverse problem in a deterministic framework. The presented results give an indication of what information we can retrieve from a tomographic estimate and tracer test data given certain information of data errors and the strength of the petrophysical relationship. In practice, we should realize the limitations of our estimate and be careful in using them (e.g., not assume that we can make an accurate inference of the correlation structure of the hydraulic conductivity structure under most circumstances). Alternatively, future work can focus on casting the problem in a stochastic framework where we parameterize the different types of errors, the uncertainty in the petrophysical relationship, and preferably estimate the hydraulic conductivity and radar velocity structure simultaneously to allow information sharing. However, the fundamental problems of estimating data errors and the uncertainty in the petrophysical relationship remain regardless of our approach to inversion.

5. ACKNOWLEDGMENTS

This research was carried out while the first author was visiting the Earth Science Division (ESD), Lawrence Berkeley National Laboratory, Berkeley, California. We want to thank ESD director Bo Bodvarsson for making this stay possible. This work was supported by the Office of Science Environmental Remediation Science Program under U.S. Dept. of Energy under Contract No. DE-AC03-76SF00098 and by the Department of Earth Sciences/Geophysics, Uppsala University.

6. REFERENCES

Alumbaugh, D., P. Y. Chang, L. Paprocki, J. R. Brainard, R. J. Glass, and C. A. Rautman (2002), Estimating moisture contents in the vadose zone using cross-borehole ground penetrating radar: A study of accuracy and repeatability, *Water Resour. Res.*, *38*, 1309, doi:10.1029/2001WR000754.

Annan, A. P. (2004), GPR Methods for Hydrogeological Studies, in *Hydrogeophysics*, edited by Y. Rubin and S. Hubbard, Chapter 7, Springer, in press.

Binley, A., G. Cassiani, R. Middleton, and P. Winship (2002), Vadose zone flow model parameterization using cross-borehole radar and resistivity imaging, *J. Hydrol.*, *267*, 147-159.

Carrera, J., and Neuman, S. P. (1986a), Estimation of aquifer parameters under transient and steady state conditions, 1, maximum likelihood method incorporating prior information, *Water Resour. Res.*, *22*, 199-210.

Carrera, J., and Neuman, S. P. (1986b), Estimation of aquifer parameters under transient and steady state conditions, 2, uniqueness, stability, and solution algorithms, *Water Resour. Res.*, *22*, 211-227.

Carrera, J., and Neuman, S. P. (1986c), Estimation of aquifer parameters under transient and steady state conditions, 3, application to synthetic and field data, *Water Resour. Res.*, *22*, 228-242.

Chen, J., S. Hubbard, and Y. Rubin (2001), Estimating the hydraulic conductivity at the South Oyster Site from geophysical tomographic data using Bayesian techniques based on the normal linear regression model, *Water Resour. Res.*, *37*, 1603-1613.

Chen, J., S. Hubbard, Y. Rubin, C. Murray, and E. Roden (2004), Geochemical characterization using geophysical data and Markov Chain Monte Carlo methods: A case study at the South Oyster Bacterial Transport Site in Virginia, *Water Resour. Res.,* in press.

Copty, N., Y. Rubin, and G. Mavko (1993), Geophysical-hydrological identification of structure permeabilities through Bayesian updating, *Water Resour. Res.*, *29*, 2813-2825.

Dagan, G. (1989), *Flow and transport in porous formations*, Springer Verlag, Berlin.

Daily, W., A. Ramirez, D. LaBrecque, and J. Nitao (1992), Electrical resistivity tomography of vadose zone water movement, *Water Resour. Res.*, *28*, 1429-1442.

Daily, W., A. Ramirez, A. Binley, and D. LaBrecque (2004), Electrical resistance tomography, *The Leading Edge*, *23*, 438-442.

Day-Lewis, F. D., J. W. Lane, J. M. Harris, and S. M. Gorelick (2003), Time-lapse imaging of saline-tracer transport in fractured rock using difference-attenuation radar tomography, *Water Resour. Res.*, *39*, 1290, doi: 10.1029/2002WR001722.

Day-Lewis, F. D., and J. W. Lane, Jr. (2004) Assessing the resolution-dependent utility of tomograms for geostatistics, *Geophys. Res. Lett.*, *31*, L07503, doi:10.1029/2004GL019617.

Deutsch, C. V., and A. G. Journel (1998), *GSLIB: A geostatistical software library and user's guide*, 2nd ed., Oxford Univ. Press, London.

Finsterle, S., (1999), iTOUGH2 user's guide, *Report LBNL-40040*, Lawrence Berkeley National Laboratory, Berkeley, California.

Gritto, R., V. A. Korneev, T. M. Daley, M. Feighner, E. L. Majer, and J. E. Peterson (2004), Surface-to-tunnel seismic tomography studies at Yucca Mountain, Nevada, *J. Geophys. Res.*, *109*, B03310, doi:10.1029/2002JB002036.

Hoeksema, R. J., and P. K. Kitanidis (1984), An application of the geostatistical approach to the inverse problem in two-dimensional groundwater modeling, *Water Resour. Res.*, 20, 1003-1020.

Hubbard, S. S., Y. Rubin, and E. Majer, 1999, Spatial correlation structure estimation using geophysical and hydro-geological data, *Water Resour. Res.*, *35*, 1809-1825.

Hubbard, S. S., J. Chen, J. Peterson, E. L. Mayer, K. H. Williams, D. J. Swift, B. Mailloux, and Y. Rubin (2001), Hydrogeological characterization of the South Oyster Bacterial Transport Site using geophysical data, *Water Resour. Res.*, *37*, 2431-2456.

Hubbard, S., and Y. Rubin, (2004), Introduction to Hydrogeophysics, in *Hydrogeophysics*, edited by Y. Rubin and S. Hubbard, Chapter 1, Springer, in press.

Hyndman, D. W., J. M. Harris, and S. M. Gorelick (1994), Coupled seismic and tracer test inversion for aquifer property characterization, *Water Resour. Res.*, *30*, 1965-1977.

Hyndman, D. W., and S. M. Gorelick (1996), Estimating lithological and transport properties in three dimensions using seismic and tracer data: the Kesterson aquifer, *Water Resour. Res.*, *32,* 2659-2670.

Hyndman, D. W., J. R. Harris, and S. M. Gorelick (2000), Inferring the relation between seismic slowness and hydraulic conductivity in heterogeneous aquifers, *Water Resour. Res.*, *36*, 2121-2132.

Lesmes, D. P. and S. Friedman (2004), Relationships between the Electrical and Hydrogeological Properties of Rocks and Soils, in *Hydrogeophysics*, edited by Y. Rubin and S. Hubbard, Chapter 4, Springer, in press.

Marquardt, D. W. (1963), An algorithm for least squares estimation of nonlinear parameters, *SIAM J. Appl. Math.*, *11*, 431-441.

McKenna, S. A., and E. P. Poeter (1995), Structure example of data fusion in site characterization, *Water Resour. Res.*, *31*, 3229-3240.

McLaughlin, D., and Townley, L. R. (1996), A reassessment of the groundwater inverse problem, *Water Resour. Res.*, *32*, 1131-1161.

Peterson, J. E., B. N. Paulsson, and T. V. McEvilly (1985), Applications of algebraic reconstruction techniques to crosshole seismic data, *Geophysics*, *50*, 1566-1580.

Peterson, J. E. (1986), The application of algebraic reconstruction techniques to geophysical problems, Ph.D. thesis, Univ. of Calif., Berkeley, California.

Peterson, J. E. (2001), Pre-inversion processing and analysis of tomographic radar data, *JEEG*, *6*, 1-18.

Prasad, M. (2003), Velocity-permeability relations within hydraulic units, *Geophysics*, *68*, 108-117.

Pride, S. R. (2004), Relationships between Seismic and Hydrological Properties, in *Hydrogeophysics*, edited by Y. Rubin and S. Hubbard, Chapter 9, Springer, in press.

Pruess, K., C. Oldenburg, and G. Moridis (1999) TOUGH2 user's guide, version 2.0, *Report LBNL-43134*, Lawrence Berkeley National Laboratory, Berkeley, California.

Scheibe, T. D. and Y. J. Chien (2003), An evaluation of conditioning data for solute transport prediction, *Ground Water*, *41*, 128-141.

Slater, L. D., A. Binley, and D. Brown (1997), Electrical imaging of fractures using ground-water salinity change, *Ground Water*, *35*, 436-442.

Slater, L., A. Binley, R. Versteeg, G. Cassiani, and R. Birken (2002), A 3D ERT study of solute transport in a large experimental tank, *J. Appl. Geophys.*, *49*, 211-229.

Spitzer, F. (1976) *Principles of Random Walk, 2nd ed.*, Springer-Verlag.

Tronicke, J., K. Holliger, Barrash, W., and M. D., Knoll (2004), Multivariate analysis of cross-hole georadar velocity and attenuation tomograms for aquifer zonation, *Water Resour. Res.*, *40*, W01519, doi:10.1029/2003WR002031.

Figure and Table captions

Figure 1. Illustration of the classification of anomalies u (a) and their relative magnitude variations α_{ij} (b) for the case where we assume several empirical relations and (c) for the case where we only assume one empirical relation.

Figure 2. We fit the cumulative concentration histories $\boldsymbol{\Psi}$ (a) measured at several sampling depths in a borehole to get a better starting model to fit the concentration histories $\boldsymbol{X}$ (b). We also show examples of cumulative concentration histories $\boldsymbol{\Psi}_0$ for an initial model (a). Each color represents the simulated data at a specific sampling location.

Figure 3. Our true hydraulic conductivity structure $\boldsymbol{Y}$ is shown in (a). We get different estimates of the hydraulic conductivity structure $\hat{\boldsymbol{Y}}$ by inverting tracer test data from a line source (b) with models constrained by the shape of the anomalies and their relative magnitude variations using different estimates of radar velocity structures that are obtained from hypothetical radar tomographic surveys between the two boreholes. We carry out these surveys for a set of radar velocity structures that have different correlations between radar velocity and hydraulic conductivity. Furthermore, we consider errors due to inaccurate zero-times of the measured travel times and errors in the acquisition geometry.

Figure 4. We calculate a series of synthetic velocity structures starting from one having a perfect linear correlation with the true hydraulic conductivity structure. The intrinsic correlation is then gradually decreased (b-j) by adding additional correlated structures until the correlation is non-existent (k).

Figure 5. Case study where the intrinsic correlation is perfect and small geophysical data acquisition errors exist (Case 1 in Table 1). The estimated velocity structure (a) has a variability that is lower than the true hydraulic conductivity structure, indicated by the vertical variograms γ_Z of the estimated velocity, the true hydraulic conductivity, and the estimated hydraulic conductivity structure of the non-stationary inversion (b), γ_Z of the estimated hydraulic conductivity structure based on the stationary inversion (c) is also shown. Our estimate based on the non-stationary inversion (d) has the correct variability (see (b)) and it is more variable than the estimate based on the stationary inversion (e). The residuals (f) and (g) for the two types of inversions show that there is no bias in the central part of the models.

Figure 6. The case where one anomaly has a different intrinsic relation, approximately at 9 to 10 m depth and 0 to 3 m along the *x*-axis. The estimated velocity structure (a) is the same as in Figure 5a. The vertical semi-variograms of the estimated velocity structure, the true hydraulic conductivity structure, and the estimate of the hydraulic conductivity structure based on the non-stationary inversion (b), and of the stationary inversion (c) show that the estimate based on the non-stationary inversion again give a correct estimate of variability and that the one based on the stationary inversion is smooth. The estimate based on the non-stationary inversion (d) accurately models the new conductive anomaly, whereas the stationary inversion (e) has an incorrect low hydraulic conductivity zone at the same location as the new conductive anomaly. The residuals of the non-stationary inversion (f) are random in the central part of the model whereas the residuals of the stationary inversion (g) have a clear bias at the new conductive anomaly.

Figure 7. Example where the intrinsic correlation is 0.63 (case 6 in Table 1). The estimated velocity structure (a) is different from the one in illustration 1 (see Figure 5a). The vertical semi-variograms of the estimated velocity structure, the true hydraulic conductivity, and the estimate based on the non-stationary inversion (b), and the stationary inversion (c) show that the non-stationary inversion gives a too variable estimate and the stationary inversion gives a too smooth estimate. Our residuals based on the non-stationary (d) and stationary inversions (e) are only approximate descriptions of the true hydraulic permeability structure, seen by the residuals (f and g) that are large, especially for the non-stationary inversion.

Figure 8. The case where we have introduced more realistic errors in the zero-times and the borehole geometry even though no borehole deviations are considered (see case 19 in Table 1). The tomogram (a) captures the major features but it is smoother than the earlier examples and the velocities are higher. The vertical semi-variograms of the estimated velocity structure, the true hydraulic conductivity, the estimate based on the non-stationary inversion (b), and the stationary inversion (c) show that both estimates of the hydraulic conductivity structure underestimates the variability, but that the non-stationary inversion estimate is more variable. Our estimates of the hydraulic conductivity structure based on the non-stationary (d) and stationary (e) inversion capture the main features of the true structure. The corresponding residuals (f and g) have some non-random behavior, especially for the non-stationary inversion.

Figure 9. We consider an unknown 2% borehole deviation (see case 20 in Table 1). The tomogram (a) is dominated by the unknown deviation, causing too high velocities and a trend of higher velocities with depth. The vertical semi-variograms of the estimated

velocity structure, the true hydraulic conductivity, the estimate based on the non-stationary inversion (b), and the stationary inversion (c) show that the non-stationary inversion estimate, probably by chance, models the variability accurately and that stationary inversion estimate is extremely smooth. The corresponding hydraulic conductivity estimates are (d and e) and the residuals (f and g) are large and show non-random behavior.

Figure 10. Criteria scores as a function of the intrinsic correlation, starting with perfect correlation for the cases where we change the intrinsic relation (Cases 1-11 in Table 1), where + specifies results of the non-stationary inversion and * specifies results of the stationary inversion. Colored arrows (solid for the non-stationary and dashed for the stationary inversions) indicate the criteria scores for a few representative cases where we consider different data acquisition errors (Cases 12-13, 15-17, and 19-20 defined in Table 1) and where the intrinsic correlation is perfect. We show (a) the normalized objective functions (criterion 1); (b) the empirical correlations (criterion 2); (c) estimated variability (criterion 4); and (d) the slopes of the empirical relation (criterion 8).

Table 1. Intrinsic correlations and data acquisition errors used in the different cases. The columns specify the values of k (see equation 20), the random horizontal errors of the transmitters and receivers within the boreholes, the error in the depth information of the receivers, errors in the horizontal separation of the wellbores, errors in the zero-times, percent deviation from vertical in one of the boreholes, the percentage of the model that has the correct anomaly type, and the number of anomalies U defined given the procedure described in Section 2.1.

Table 2. We give the criteria scores defined in section 2.4 (Cr1-Cr9) for all Cases and for both the non-stationary (NS) and stationary (S) inversion estimates of the hydraulic conductivity structure.

Case	*k*	*Max. horizontal random deviation within boreholes (cm)*	*Error in the depth of receivers (cm)*	*Error in the horizontal separation of wellbores (cm)*	*Zero time error (ns)*	*Deviation from vertical (%)*	*Correct anomaly type (%)*	*U*
1	1.	2	0	0	0.33	0	90	7
2	0.9	2	0	0	0.33	0	90	7
3	0.8	2	0	0	0.33	0	93	7
4	0.7	2	0	0	0.33	0	92	6
5	0.6	2	0	0	0.33	0	90	8
6	0.5	2	0	0	0.33	0	84	10
7	0.4	2	0	0	0.33	0	76	11
8	0.3	2	0	0	0.33	0	70	9
9	0.2	2	0	0	0.33	0	61	9
10	0.1	2	0	0	0.33	0	56	12
11	0.0	2	0	0	0.33	0	49	10
12	1.0	2	0	-10	0.33	0	90	6
13	1.0	2	0	-50	0.33	0	77	7
14	1.0	2	-1	0	0.33	0	89	8
15	1.0	2	-5	0	0.33	0	91	4
16	1.0	2	-15	0	0.33	0	83	3
17	1.0	2	0	0	1	0	90	5
18	1.0	2	0	0	3	0	92	8
19	1.0	2	-5	-10	1	0	90	5
20	1.0	2	0	0	0.33	2	74	4

Table 1
Linde et al.

Case	$\Phi_{conc}/\Phi_{conc}^{perfect}$ $\times 10^{-3}$ *Cr1*	$\rho(Y, \hat{V})$ *Cr2*	$Y_{eff} - \hat{Y}_{ef}$ *Cr3*	$\sigma_{\hat{Y}} / \sigma_Y$ *Cr4*	$\varsigma(Y, \hat{Y})$ *Cr5*	$L_1(Y, \hat{Y})$ *Cr6*	$\hat{b}/b$ *Cr7*	$L_1(\hat{a}_u - \hat{a}_{mean})$ *Cr8*	$L_1(l_i - \hat{l}_i)$ *Cr9*
1_{NS}	3.0	0.62	-0.022	97	-0.028	0.17	3.49	0.81	0.016
1_S	29	0.85	-0.007	74	-0.034	0.13	0.87	-	0.014
2_{NS}	7.2	0.72	-0.009	90	-0.021	0.16	2.86	0.39	0.014
2_S	31	0.85	-0.009	74	-0.037	0.13	0.88	-	0.014
3_{NS}	41	0.50	-0.026	114	-0.011	0.24	5.69	1.07	0.018
3_S	37	0.84	-0.031	74	-0.061	0.14	0.89	-	0.029
4_{NS}	37	0.70	-0.051	87	-0.071	0.19	3.48	0.46	0.027
4_S	50	0.81	-0.015	70	-0.047	0.14	0.91	-	0.015
5_{NS}	26	0.56	-0.044	107	-0.040	0.22	3.51	0.46	0.035
5_S	68	0.75	-0.022	71	-0.053	0.16	0.91	-	0.017
6_{NS}	21	0.44	-0.054	130	-0.022	0.24	4.46	1.84	0.042
6_S	110	0.65	-0.029	68	-0.064	0.18	0.87	-	0.021
7_{NS}	6.6	0.37	-0.082	106	-0.084	0.27	6.26	4.6	0.072
7_S	160	0.49	-0.039	65	-0.077	0.20	0.89	-	0.024
8_{NS}	33	0.17	-0.088	1.31	-0.059	0.35	5.77	1.75	0.054
8_S	220	0.29	-0.046	0.63	-0.087	0.23	0.94	-	0.028
9_{NS}	32	0.03	-0.163	1.84	-0.062	0.41	21.5	4.51	0.079
9_S	430	-0.06	-0.000	0	-0.043	0.26	-0.90	-	0.047
10_{NS}	180	0.12	-0.032	1.37	0.0124	0.36	-7.30	4.35	0.068
10_S	370	0.11	-0.004	0.43	-0.053	0.24	-0.77	-	0.043
11_{NS}	290	0.13	-0.045	1.09	-0.039	0.34	-5.19	1.66	0.046
11_S	260	0.11	-0.038	0.38	-0.094	0.21	0.82	-	0.024
12_{NS}	16	0.59	-0.041	0.89	-0.057	0.20	2.01	0.22	0.030
12_S	42	0.79	-0.022	0.85	-0.040	0.15	0.99	-	0.019
13_{NS}	146	0.43	-0.132	1.76	-0.040	0.37	12.5	3.29	0.042
13_S	260	0.56	-0.038	0.38	-0.094	0.21	0.82	-	0.024
14_{NS}	20	0.65	-0.002	0.28	-0.019	0.18	2.77	1.11	0.021
14_S	42	0.84	-0.012	0.71	-0.042	0.14	0.88	-	0.014
15_{NS}	10	0.80	-0.015	0.22	-0.039	0.16	1.47	0.18	0.019
15_S	11	0.83	-0.000	0.68	-0.032	0.14	0.93	-	0.016
16_{NS}	28	0.67	0.002	0.17	-0.035	0.18	1.00	6.23	0.025
16_S	22	0.72	0.011	0.60	-0.027	0.17	1.29	-	0.022
17_{NS}	20	0.76	0.006	0.20	-0.021	0.17	2.37	0.72	0.013
17_S	34	0.84	-0.009	0.71	-0.039	0.14	0.90	-	0.014
18_{NS}	22	0.38	-0.106	0.32	-0.087	0.24	8.97	3.58	0.028
18_S	41	0.81	-0.010	0.65	-0.044	0.15	1.04	-	0.015
19_{NS}	18	0.78	-0.034	0.76	-0.063	0.17	1.76	0.51	0.015
19_S	19	0.80	-0.032	0.50	-0.080	0.17	0.77	-	0.021
20_{NS}	66	0.41	-0.092	1.02	-0.100	0.27	2.38	1.10	0.021
20_S	100	0.51	-0.073	0.30	-0.140	0.23	0.33	-	0.026

Table 2
Linde et al.

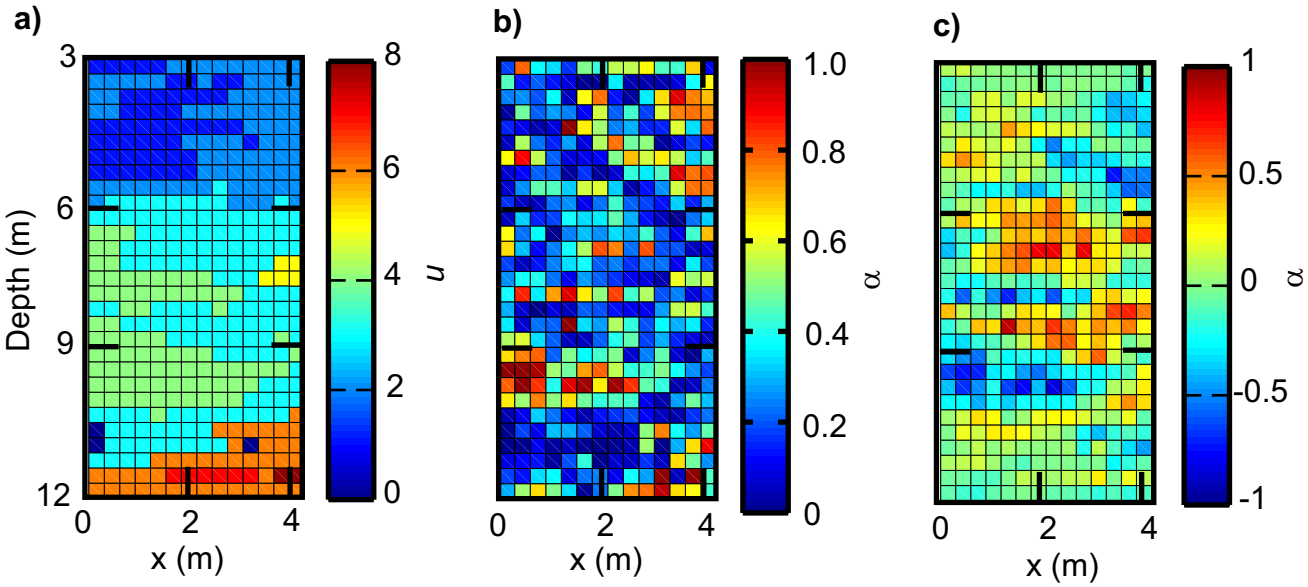

Linde et al.
Figure 1

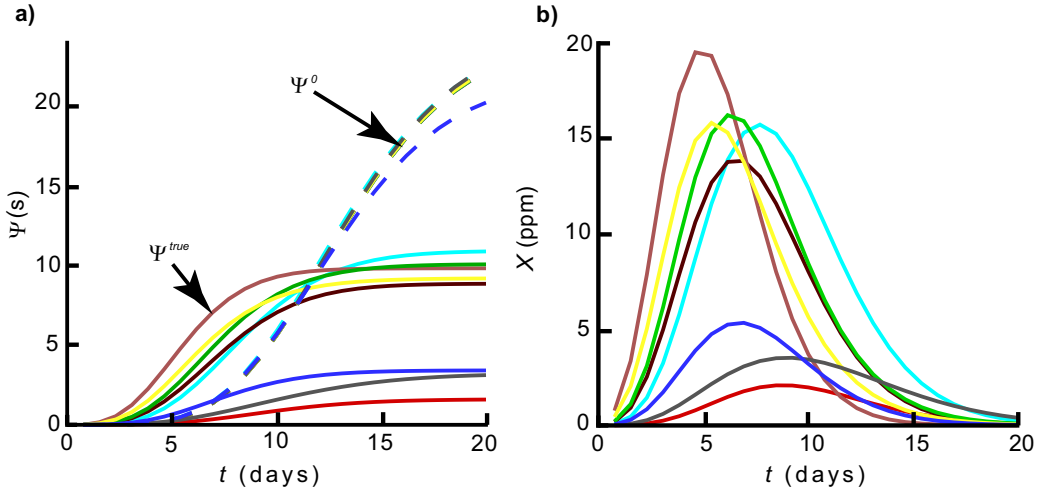

Figure 2
Linde et al.

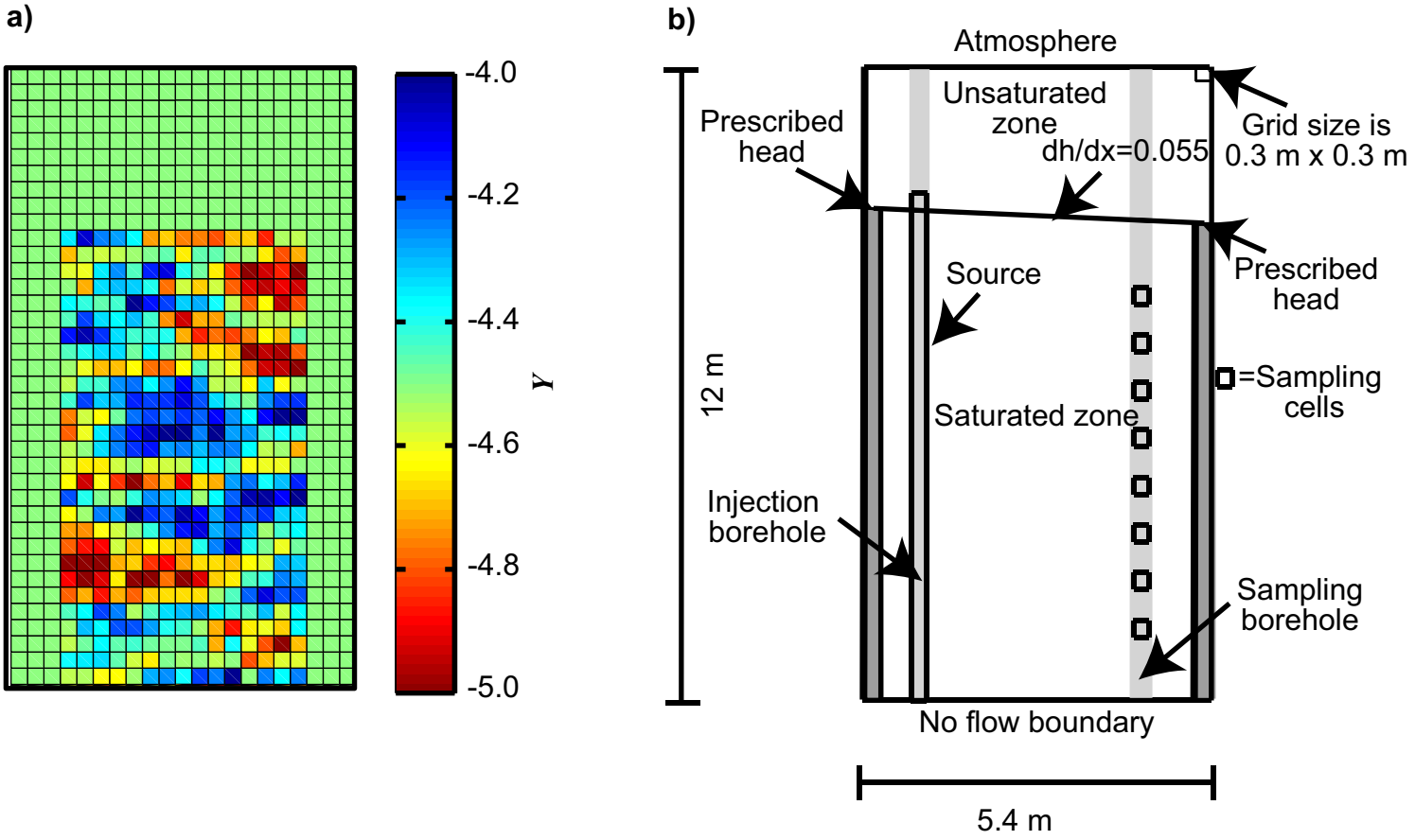

Linde et al.
Figure 3

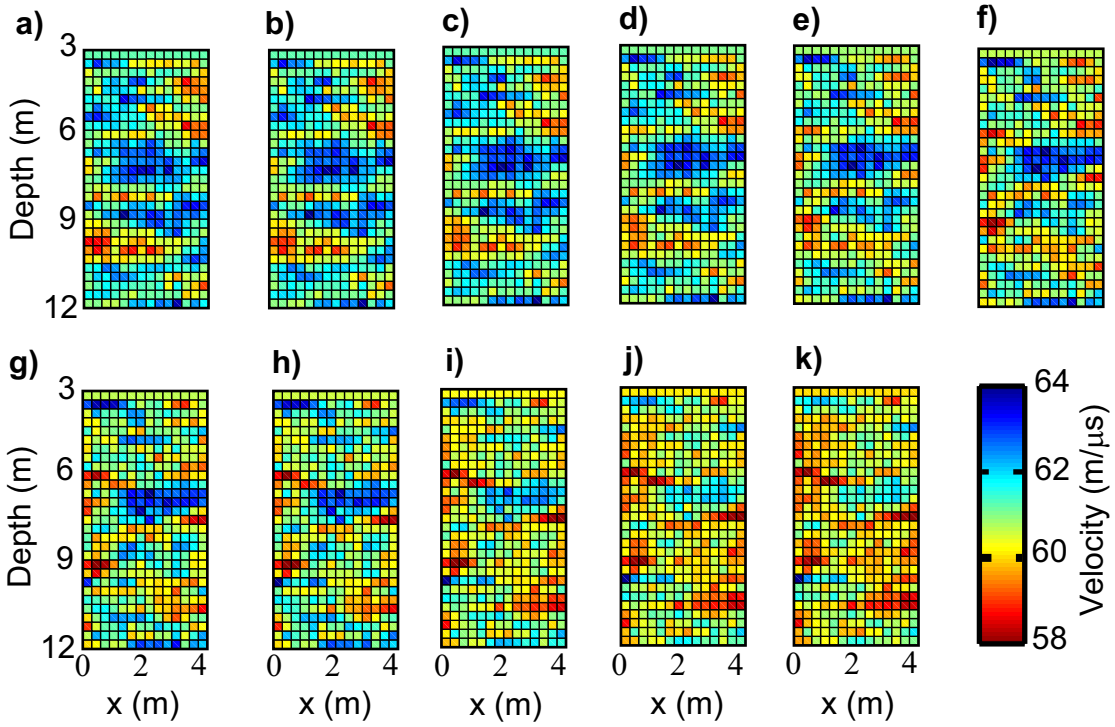

Linde et al.
Figure 4

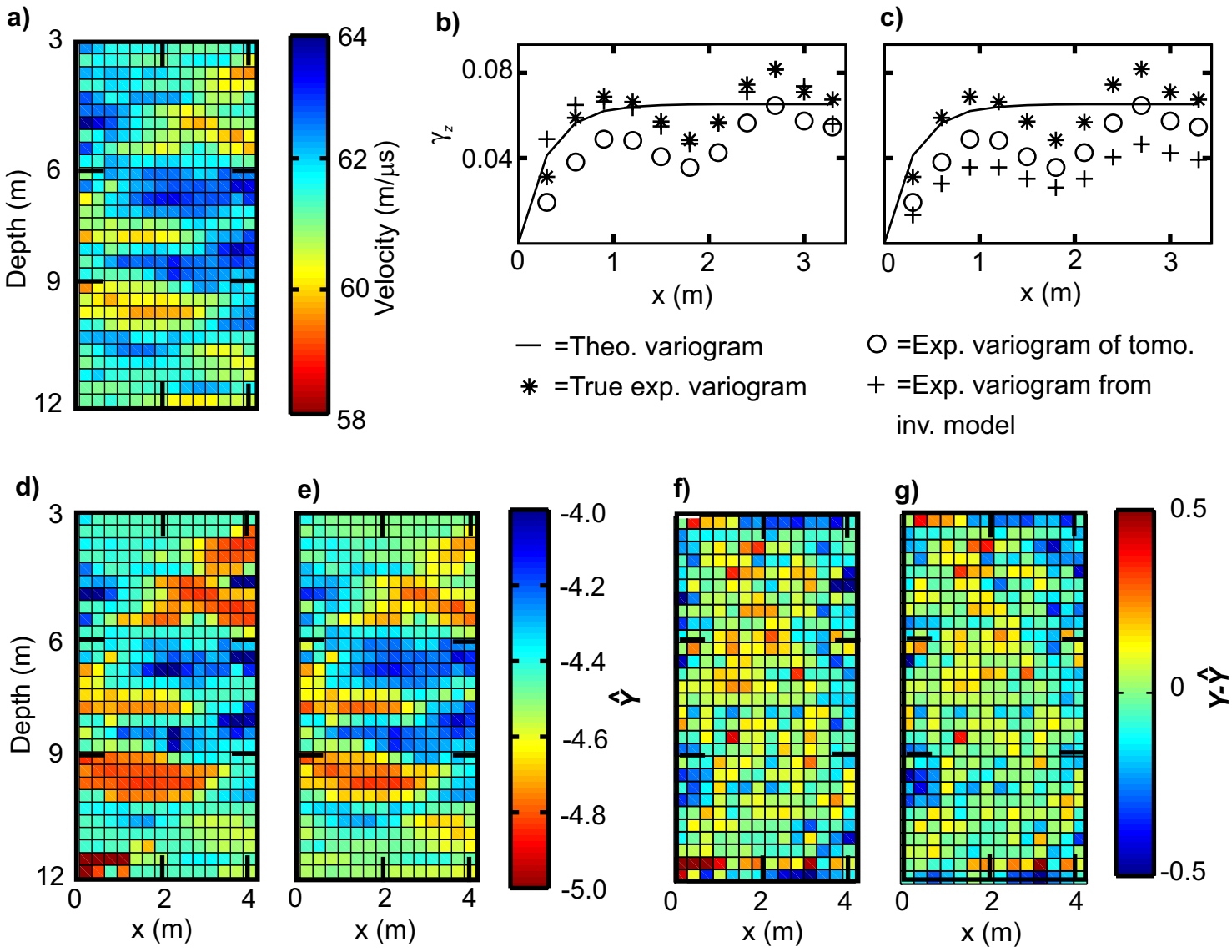

Linde et al.
Figure 5

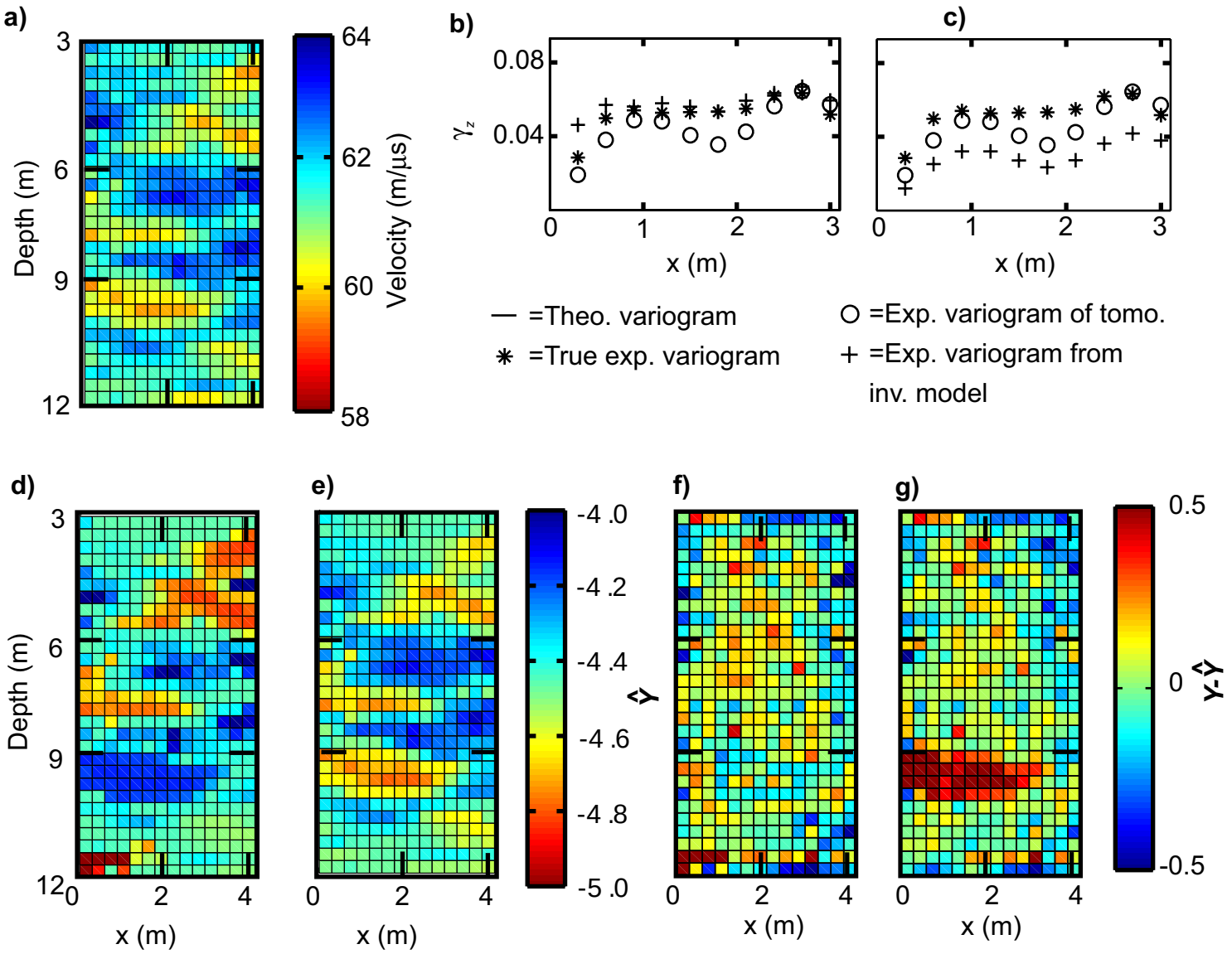

Linde et al.
Figure 6

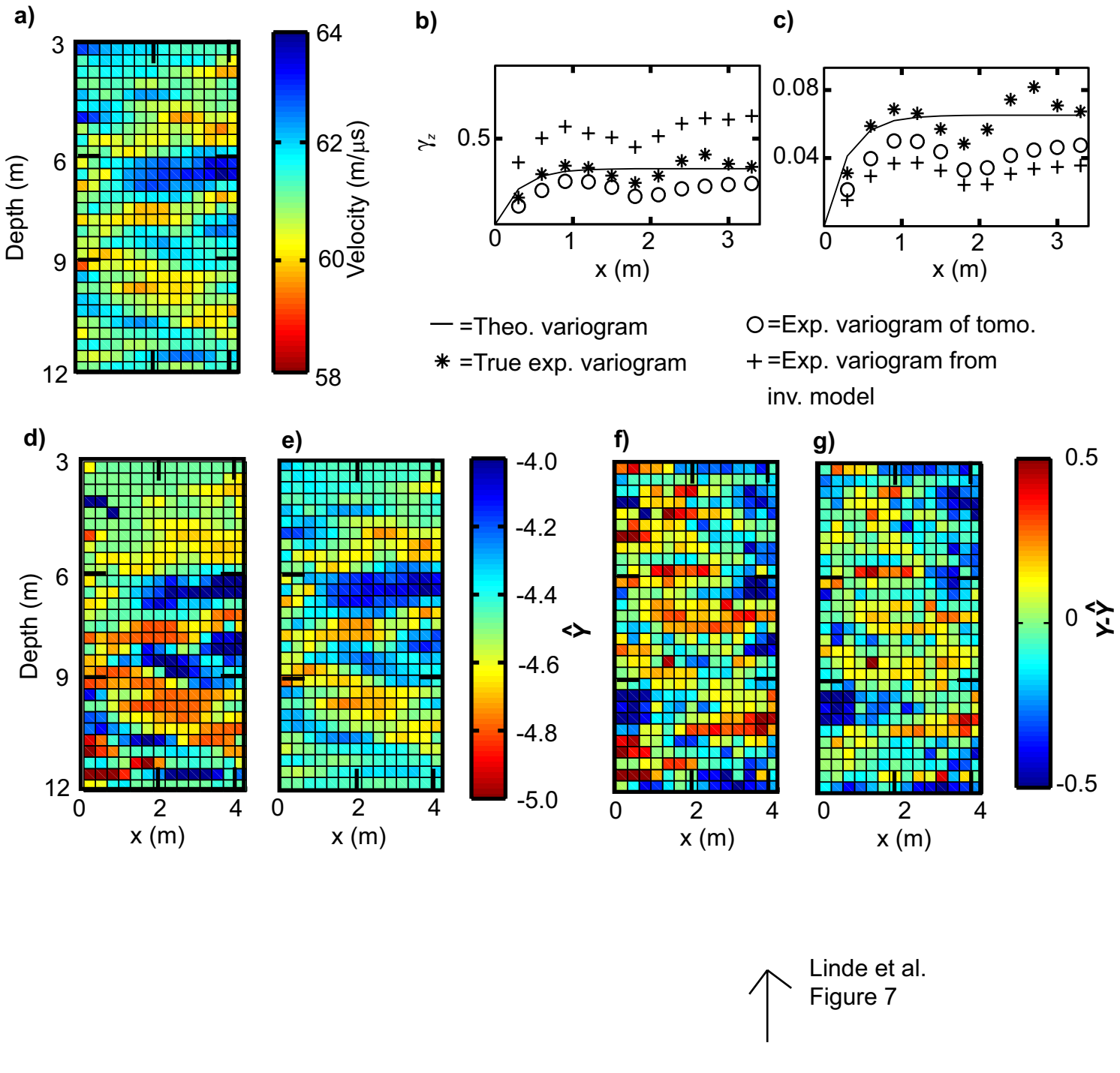

Linde et al.
Figure 7

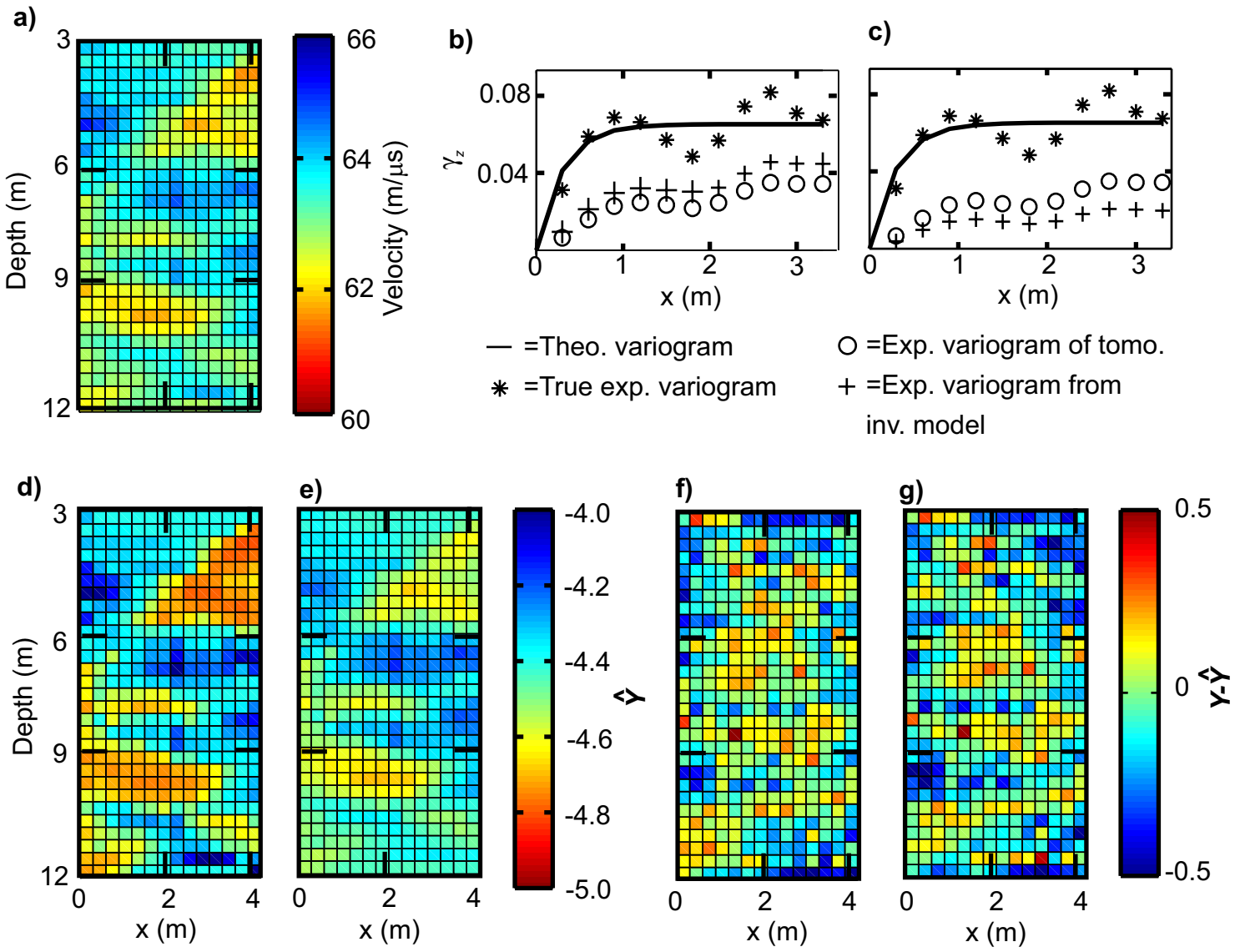

Linde et al.
Figure 8

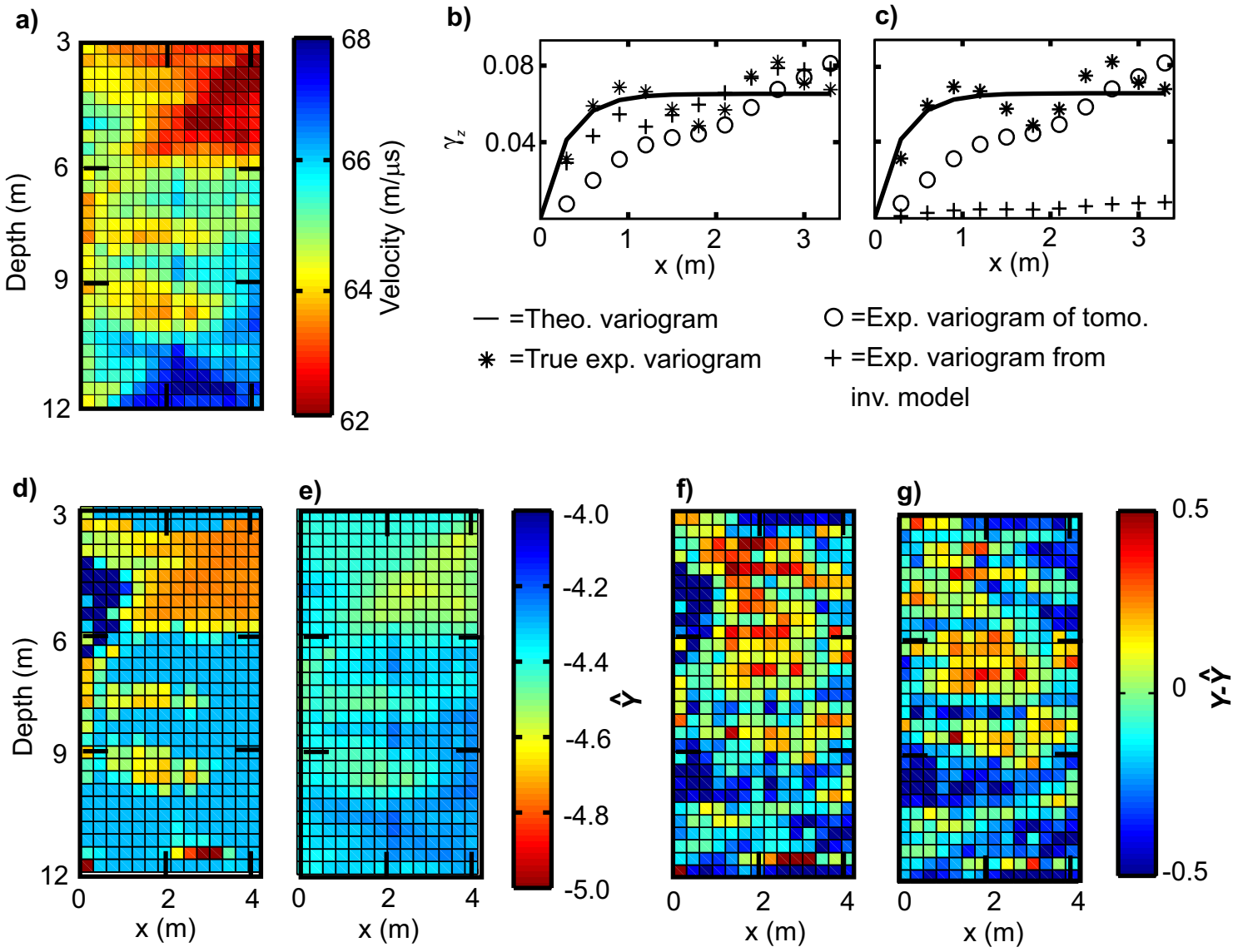

Linde et al.
Figure 9

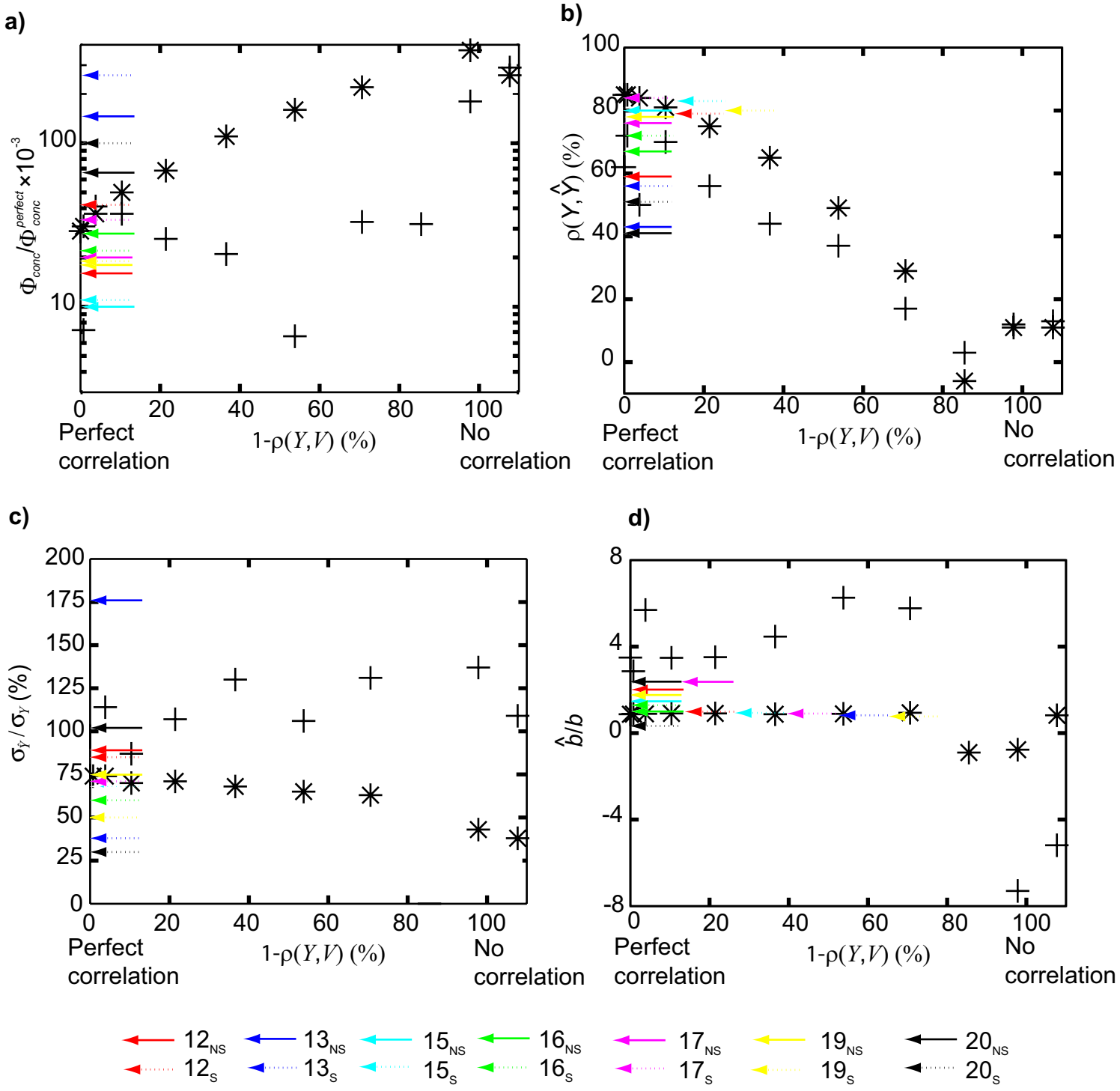

Linde et al.
Figure 10